Leaky ryanodine receptors contribute to diaphragmatic weakness during mechanical ventilation

Stefan Matecki[a,1], Haikel Dridi[a,1], Boris Jung[a,b], Nathalie Saint[a], Steven R. Reiken[c,d,e], Valérie Scheuermann[a], Ségolène Mrozek[a], Gaetano Santulli[c,d,e], Alisa Umanskaya[c,d,e], Basil J. Petrof[f], Samir Jaber[a,b], Andrew R. Marks[c,d,e,2], and Alain Lacampagne[a,2]

[a]Inserm U1046, CNRS UMR 91214, Université de Montpellier, Centre Hospitalier Regional Universitaire de Montpellier, 34295 Montpellier, France; [b]Department of Anesthesiology and Critical Care Medicine, St. Eloi Teaching Hospital, 34295 Montpellier, France; [c]Department of Physiology and Cellular Biophysics, College of Physicians and Surgeons, Columbia University, New York, NY 10032; [d]The Clyde and Helen Wu Center for Molecular Cardiology, College of Physicians and Surgeons, Columbia University, New York, NY 10032; [e]Department of Medicine, College of Physicians and Surgeons, Columbia University, New York, NY 10032; and [f]Meakins-Christie Laboratories, McGill University and McGill University Hospital Research Institute, Montreal, QC H2X 2P2, Canada

Edited by David E. Clapham, Harvard Medical School, Boston, MA, and approved June 29, 2016 (received for review March 1, 2016)

Ventilator-induced diaphragmatic dysfunction (VIDD) refers to the diaphragm muscle weakness that occurs following prolonged controlled mechanical ventilation (MV). The presence of VIDD impedes recovery from respiratory failure. However, the pathophysiological mechanisms accounting for VIDD are still not fully understood. Here, we show in human subjects and a mouse model of VIDD that MV is associated with rapid remodeling of the sarcoplasmic reticulum (SR) Ca^{2+} release channel/ryanodine receptor (RyR1) in the diaphragm. The RyR1 macromolecular complex was oxidized, S-nitrosylated, Ser-2844 phosphorylated, and depleted of the stabilizing subunit calstabin1, following MV. These posttranslational modifications of RyR1 were mediated by both oxidative stress mediated by MV and stimulation of adrenergic signaling resulting from the anesthesia. We demonstrate in the murine model that such abnormal resting SR Ca^{2+} leak resulted in reduced contractile function and muscle fiber atrophy for longer duration of MV. Treatment with β-adrenergic antagonists or with S107, a small molecule drug that stabilizes the RyR1–calstabin1 interaction, prevented VIDD. Diaphragmatic dysfunction is common in MV patients and is a major cause of failure to wean patients from ventilator support. This study provides the first evidence to our knowledge of RyR1 alterations as a proximal mechanism underlying VIDD (i.e., loss of function, muscle atrophy) and identifies RyR1 as a potential target for therapeutic intervention.

excitation–contraction coupling | beta adrenergic signaling | calcium | VIDD | skeletal muscle

The need for respiratory support by controlled mechanical ventilation (MV) is one of the main reasons for admission to intensive care units (ICUs). Although it is life saving in the short term, human and animal studies have shown that MV results in a progressive reduction in diaphragmatic force-generating capacity, together with diaphragm muscle fiber injury and atrophy (1, 2). These findings comprise a condition termed ventilator-induced diaphragmatic dysfunction (VIDD) (3), which is common in an ICU setting (4), and can interfere with the ability to discontinue MV (5), with a major negative impact on patient outcomes and increased health care costs (6). The precise pathways involved in MV-induced diaphragm weakness remain partially understood. Animal models suggest that oxidative stress plays a major role in VIDD (7, 8) and recent studies have identified mitochondria as an essential source of reactive oxygen species (ROS) implicated in VIDD (9, 10). ROS production is linked to activation of proteolytic systems such as caspases and calpains (11), which play significant roles in degrading cytoskeletal proteins in muscle (6, 12, 13) directly involved in the development of MV-induced diaphragm muscle fiber atrophy and injury (7, 14, 15). Despite many of the processes implicated in VIDD having been associated with increased oxidative stress (16), other mechanisms could also be involved. Indeed, in ICU, many situations including anesthetics, MV, sepsis, or pain may induce an overstimulation of the adrenergic response, leading to increased catecholamine synthesis (17, 18). Albeit elevated levels of circulating endogenous catecholamines have been associated to a generalized myopathy process in animal models (19), and higher mortality in ICUs (18), whether catecholamine release during MV may impair diaphragm function is unknown. Similarly, the potential role of Ca^{2+} homeostasis disruption in VIDD has never been addressed. We recently observed a reduction of diaphragmatic force production after only 6 h of MV in mice, in absence of atrophy or histological injury (20). We hypothesized that such uncoupling between functional and histological parameters of VIDD could be explained by defects in Ca^{2+} homeostasis and excitation–contraction coupling at an early stage of VIDD and, if so, might lend itself to early preventive intervention. Furthermore, because deregulated Ca^{2+} homeostasis can lead to activation of caspases and calpains (16), this impaired Ca^{2+} signaling could also help to account for the subsequent development of diaphragm muscle atrophy and injury. In skeletal muscle, normal excitation–contraction coupling entails activation of voltage-sensing Ca^{2+} channels in the transverse tubules that, in turn, activate the sarcoplasmic reticulum (SR) Ca^{2+}

Significance

Ventilator-induced diaphragmatic dysfunction (VIDD) refers to the diaphragm muscle weakness that follows prolonged controlled mechanical ventilation, impeding recovery from respiratory failure. The mechanisms underlying VIDD are still not fully understood. Using human samples and murine models of VIDD, we identify here a pathophysiological pathway involving structural and functional impairment of the ryanodine receptor (RyR1), the main sarcoplasmic reticulum (SR) Ca^{2+} release channel. We demonstrate that RyR1 defects, which contribute to diaphragm muscle weakness, induced by controlled mechanical ventilation are the result of oxidative stress associated to sympathetic nervous system activation. Thus, preventing RyR1-mediated SR Ca^{2+} leak may provide a novel therapeutic approach in controlled mechanical ventilation.

Author contributions: S. Matecki, S.J., A.R.M., and A.L. designed research; S. Matecki, H.D., N.S., V.S., and S.J. performed research; S.R.R., G.S., and A.U. contributed new reagents/analytic tools; B.J., S. Mrozek, G.S., B.J.P., S.J., and A.L. analyzed data; and S. Matecki, G.S., B.J.P., S.J., A.R.M., and A.L. wrote the paper.

Conflict of interest statement: A.R.M. is on the scientific advisory board and the board of directors and owns shares in ARMGO Pharma, Inc., a start-up company developing RyR-targeted drugs for clinical use in the treatment of cardiac and muscle dysfunction.

This article is a PNAS Direct Submission.

[1]S. Matecki and H.D. contributed equally to this work.

[2]To whom correspondence may be addressed. Email: arm42@cumc.columbia.edu or alain.lacampagne@inserm.fr.

This article contains supporting information online at www.pnas.org/lookup/suppl/doi:10.1073/pnas.1609707113/-/DCSupplemental.

release channel/ryanodine receptor (RyR1) (21). RyR1-dependent Ca^{2+} release triggers actin-myosin cross-bridge formation and, hence, muscle contraction (21). RyR1 is a homotetrameric macromolecular protein complex that includes four RyR1 monomers (~565 kDa each), kinases, a phosphatase (PP1), a phosphodiesterase (PDE4D3), and calmodulin (21), The RyR1 channel-stabilizing subunit calstabin1 (Cal1 or FK506 binding protein 12, FKBP12) is critical to the proper function of the channel (22). Maladaptive cAMP-dependent protein kinase A (PKA)-mediated phosphorylation and redox-dependent modifications (cysteine-nitrosylation and oxidation) of RyR1 have been linked to a loss of the normal association between calstabin1 and the rest of the complex (23, 24). This RyR1 remodeling, in turn, results in impaired Ca^{2+} handling with abnormal Ca^{2+} leak from the SR and associated contractile dysfunction in conditions as diverse as heart failure, chronic muscle fatigue, muscular dystrophy, and aging (25–28). In the present study, we postulated that early MV-induced oxidative stress and catecholamine release synergistically affect the diaphragm RyR1 complex and impair Ca^{2+} homeostasis, thereby leading to SR Ca^{2+} leak, reduced tetanic Ca^{2+}, and eventually leading to the development of VIDD.

Results

Increased RyR1 Open Probability in Diaphragm Fibers Correlates with VIDD. To evaluate the remodeling and functional abnormalities of RyR1 in the diaphragm of human patients subjected to MV, we obtained diaphragm biopsies from brain-dead organ donor patients who had undergone long-term MV (98 ± 65 h) immediately before organ harvest. We compared these specimens to diaphragm biopsies from short-term MV (2.3 ± 0.4 h) patients, obtained during thoracic surgery for removal of solitary lung nodules (see Table S1 for patients description). SR fractions were purified to analyze the biochemical properties of the RyR1 macromolecular complex (Fig. 1 *A* and *B*). RyR1 immunoprecipitation after long-term MV revealed a significant increase in RyR1 oxidation, S-nitrosylation, Ser-2844 phosphorylation, and calstabin1 dissociation. This biochemical remodeling of the RyR1 channels is known as the "biochemical signature" of "leaky" RyR1 channels (21). It was associated with a significant increase in RyR1 open probability (P_O) compared with controls short-term MV measured in channels incorporated in planar lipid bilayers in conditions under which normal nonremodeled RyR1 channels are tightly closed (P_O = ~0) (Fig. 1 *C* and *D*). This elevated P_O is consistent with increased SR Ca^{2+} leak.

Defective RyR1 Function Is an Early Pathophysiological Event in VIDD. One limitation of human samples is the potential influence of comorbidities and confounding factors associated with critical illness. Moreover, histological damage in human muscle fibers could account for both the reduction in diaphragmatic force production and RyR1 remodeling (2). Therefore, to examine early events in the course of VIDD, we took advantage of a mouse model that exhibits a significant loss of diaphragmatic force-generating capacity after only 6 h of MV (Fig. 2 *A* and *B*). We evaluated RyR1 remodeling in the mechanically ventilated diaphragm before the onset of histological alterations associated with the later stages of VIDD (20). MV-induced diaphragm muscle weakness in mice was associated with significant RyR1 remodeling consisting of RyR1 S-nitrosylation, oxidation, Ser-2844 phosphorylation, and calstabin1 dissociation (Fig. 2 *C* and *D*). RyR1 functional properties were next evaluated in situ by measuring spontaneous SR Ca^{2+} release events (i.e., Ca^{2+} sparks). A significant increase in spontaneous Ca^{2+} sparks frequency reflects increased RyR1-mediated SR Ca^{2+} leak (27, 28). After 6 h of MV, Ca^{2+} sparks frequency was significantly increased in diaphragm fibers (Fig. 2 *E* and *F*). Because MV induces oxidative stress in the diaphragm, and antioxidant treatment has been reported to prevent VIDD, a group of mice was continuously injected with Trolox, a permeable analog of vitamin E used as an antioxidant scavenger (8, 29, 30). As reported in rats mechanically

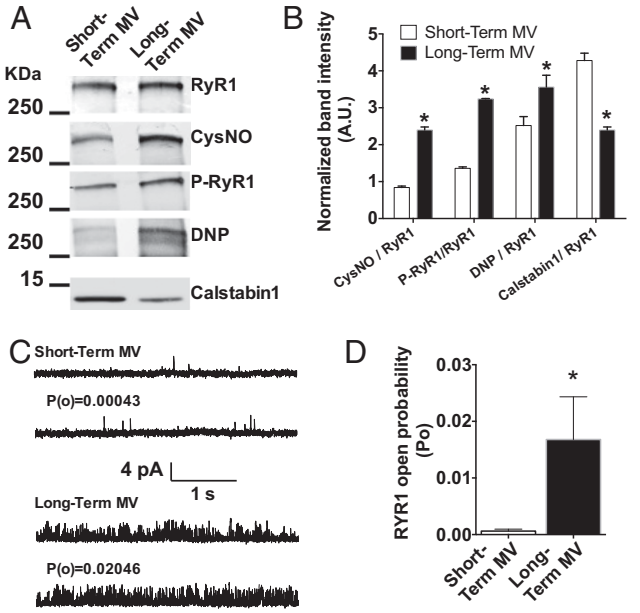

Fig. 1. VIDD is associated with defective RyR1 in human diaphragm muscle. Representative immunoblots (*A*) of immunoprecipitated RyR1 from human diaphragm samples collected after short-term (control) and long-term (MV) controlled mechanical ventilation in humans (Table S1). (Each blot corresponds to adjacent wells of the same gel.) Bar graphs (*B*) show quantification of immunoblots, relative to total RyR1 (mean ± SEM, n = 10 and 9 in control and MV, respectively, $^*P < 0.05$, MV vs. control). CysNO, thio-nitrosylation; DNP, 2,4-dinitrophenylhydrazone; P^-RyR1, phosphorylated RyR1 (at serine 2844). (*C*) Single-channel traces of RyR1 incorporated in planar lipid bilayers with 150 nM Ca^{2+} in the cis chamber, corresponding to representative experiments performed with human diaphragm biopsies from short-term and long-term MV groups. (*D*) Controlled mechanical ventilation increases RyR1 P_O: Mean P_O was 0.0006 ± 0.0003 in control (n = 18), and after MV, the P_O increased to 0.0167 ± 0.00754 (n = 40).

ventilated for 12 h (29), Trolox treatment in mice ventilated for 6 h prevented MV-induced diaphragm muscle weakness (Fig. 2*B*). In addition, we observed that Trolox prevented MV-induced RyR1 biochemical remodeling (Fig. 2 *C* and *D*) and the associated increase in Ca^{2+} sparks frequency (Fig. 2 *E* and *F*). Interestingly, this RyR1 leak was due to MV only, because non-MV mice that were identically intubated, anesthetized, and immobilized for 6 h but maintained on a spontaneous breathing mode of respiration with 4 cmH_20 of continuous positive airway pressure (CPAP mode) did not demonstrate profound biochemical remodeling of diaphragm RyR1 (Fig. 3 *A* and *B*). Besides, compared with MV samples, CPAP samples did not exhibit Calstabin1 depletion or RyR1 oxidation. They were, however, similarly phosphorylated. No functional alteration of the channel complex, as indicated by a normal Ca^{2+} sparks frequency, was found in non-MV anesthetized mice (Fig. 3*C*) and no muscle weakness could be observed (Fig. 3*D*) as reported (20).

Role of β-Adrenergic Signaling Pathway in VIDD. As emphasized above, critical illness and anesthesia may result in overstimulation of the adrenergic system. The expression pattern of β-adrenergic receptors was assessed by immunoblot in the diaphragm, which expresses predominantly β2 isoform and β1 in a lower proportion (Fig. 4*A*). To address the role of β-adrenergic receptors in VIDD, mice were ventilated for 6 h in the presence of the nonselective β1-β2 receptors antagonist, propranolol, or with the selective β2 antagonist, ICI118551 (31). Both beta blockers prevented the diaphragm weakness after 6 h of MV (Fig. 4*B*). This effect was also accompanied by a lower remodeling of the RyR1 complex. Both propranolol and ICI118551 prevented calstabin1 depletion and S2844-RYR1, whereas RyR1 oxidation persisted (Fig. 4*C*). To

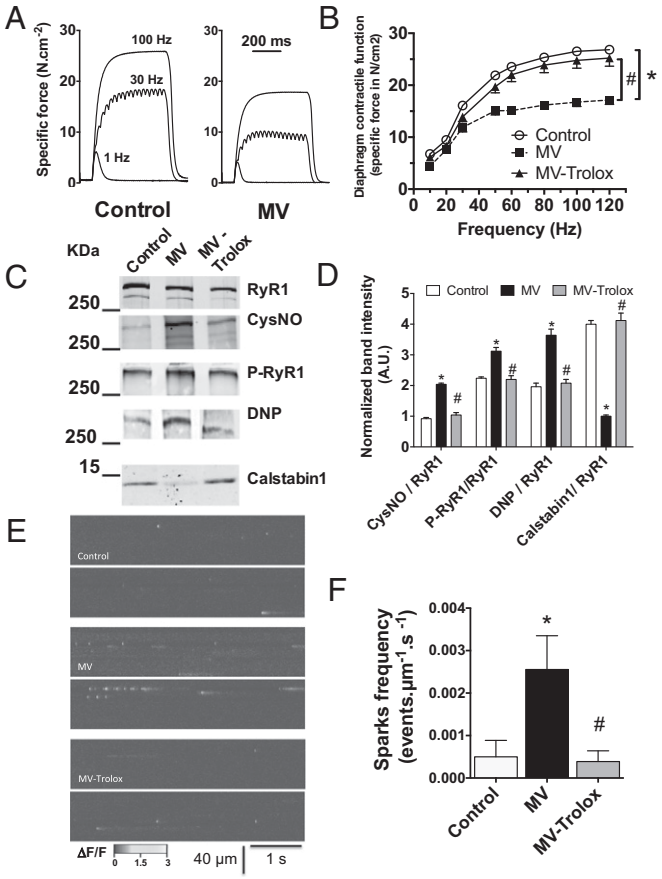

Fig. 2. RyR1 mediated SR Ca^{2+} leak in murine diaphragm muscle after 6 h of MV. (*A*) Representative records of diaphragmatic specific force production measured ex vivo at 1, 30, and 100 Hz in muscle bundles under isometric conditions in control and under controlled mechanical ventilation during 6 h (MV, 6 h) mice. (*B*) Average force–frequency relationships recorded in control ($n = 8$), mechanically ventilated for 6 h (MV, $n = 10$), mechanically ventilated for 6 h and treated with Trolox (MV-trolox, $n = 8$) groups. Representative immunoblots (each blot corresponds to adjacent wells of the same gel) of immunoprecipitated RyR1 (*C*) and bar graphs (*D*) showing quantification of proteins relative to total RyR1 immunoprecipitated from murine diaphragm samples collected in control, MV, and MV-Trolox groups. CysNO, thio-nitrosylation; DNP, 2,4-dinitrophenylhydrazone; P*RyR1, phosphorylated RyR1 (at serine 2844). Spontaneous SR Ca^{2+} release events were recorded in fluo-4-loaded permeabilized diaphragm fibers by laser scanning confocal microscopy. (*E*) Representative $\Delta F/F$ line-scan images (1.54 ms per line) recorded in control, after MV and after MV with Trolox treatment. (*F*) Mean Ca^{2+} sparks frequency was used as an index of resting SR Ca^{2+} leak. Results are expressed as mean ± SEM (*$P < 0.05$, MV vs. control; #$P < 0.05$, MV-Trolox vs. MV).

account for RyR1 phosphorylation, PKA activity was measured in diaphragm samples after 1, 2, 3, and 6 h of ventilation and compared with a maximal level of PKA stimulation obtained by injecting isoproterenol (3 mg/kg) 30 min before euthanizing the mice (Fig. 4*D*). PKA activity increased after 1 h of MV to reach a plateau between 2 and 6 h that was not significantly different from the maximal level. When the animals were treated with ICI118551 (10 mg/kg) during the MV, the level of PKA activity was significantly reduced and was similar to the basal level obtained by treating control animals with ICI118551 (10 mg/kg).

RyR1 Is a Potential Therapeutic Target in VIDD. To directly target RyR1 and, thus, assess its role as a major pathophysiological target in VIDD, we treated mechanically ventilated mice with the rycal S107. Rycals are small orally available agents known to prevent depletion of calstabin1 from the RyR1 complex despite PKA phosphorylation, S-nitrosylation, and/or oxidation of RyR1 (27, 28). Consistently, in mice, S107 prevented depletion of calstabin1 from RyR1 macromolecular complex without protecting against RyR1 oxidation and phosphorylation (Fig. 5 *A* and *B*). In addition, S107 prevented the loss of diaphragmatic force-generating capacity induced by MV (Fig. 5*C*) and the increase in Ca^{2+} spark frequency (Fig. 5*D*). These data suggest that reducing RyR1-mediated SR Ca^{2+} leak with S107 improves diaphragmatic muscle force production.

Evaluation of the Diaphragm After 12 H of MV. The hallmarks of VIDD are muscle atrophy and impaired contractility (2). With 6 h of ventilation in mice, we are able to reproduce the loss of force production without any histological damage (20). To further evaluate the role of RyR1 in VIDD, we evaluated diaphragm histological characteristics (i.e., fiber cross-sectional area, fiber type distribution) and force production following 12 h of MV. The mean cross-sectional area of all diaphragm fibers was significantly reduced compared with control animals (Fig. 6 *A*, *B*, and *G*). There was no significant alteration in the proportions of type I (slow twitch) and type II (fast twitch) (Fig. 6 *A* and *B* and Fig. S1). A significant reduction in force production (Fig. 6 *H* and *I*) accompanied this atrophy after 12 h of ventilation. Interestingly, treatments with the specific β2 antagonist ICI118-551 or S107 prevented both muscle fiber atrophy and loss of contractility. It is to note that none of the treatments had any effect on fiber size or force production in control condition.

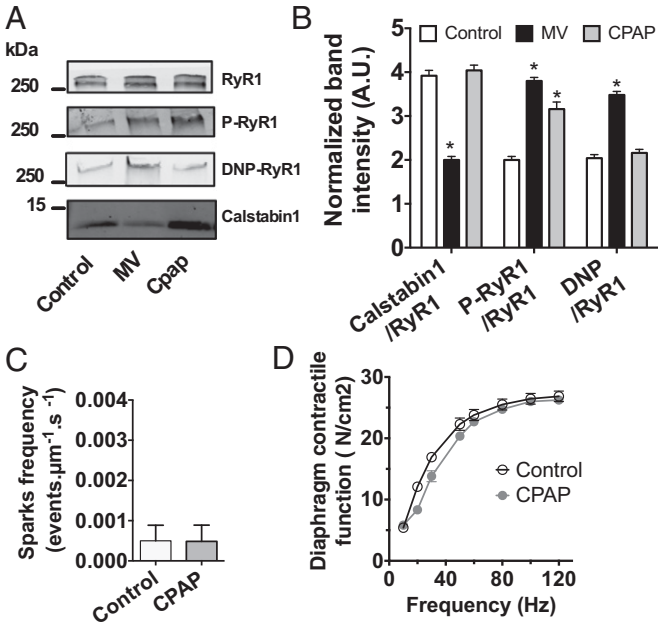

Fig. 3. Ventilation in CPAP mode does not affect RyR1 remodeling. Representative immunoblots (*A*) of immunoprecipitated RyR1 from mouse diaphragm samples collected in control condition (control) or after 6 h of controlled mechanical ventilation or continuous positive pressure (MV or CPAP). (Each blot corresponds to adjacent wells of the same gel.) Bar graphs (*B*) show quantification of immunoblots, relative to total RyR1. Results are expressed as mean ± SEM, $n = 10$ in control and 5 in MV and CPAP (*$P < 0.05$ vs. control). (*C*) Spontaneous SR Ca^{2+} release events were recorded in fluo-4-loaded permeabilized diaphragm fibers by laser scanning confocal microscopy in control and CPAP condition. Mean Ca^{2+} sparks frequency used, as an index of resting SR Ca^{2+} leak, was not significantly different between CPAP and control mice. (control $n = 7$, CPAP $n = 6$). (*D*) Average specific force–frequency relationships recorded in diaphragm muscle in control and after 6 h of CPAP (control $n = 7$, CPAP, $n = 6$).

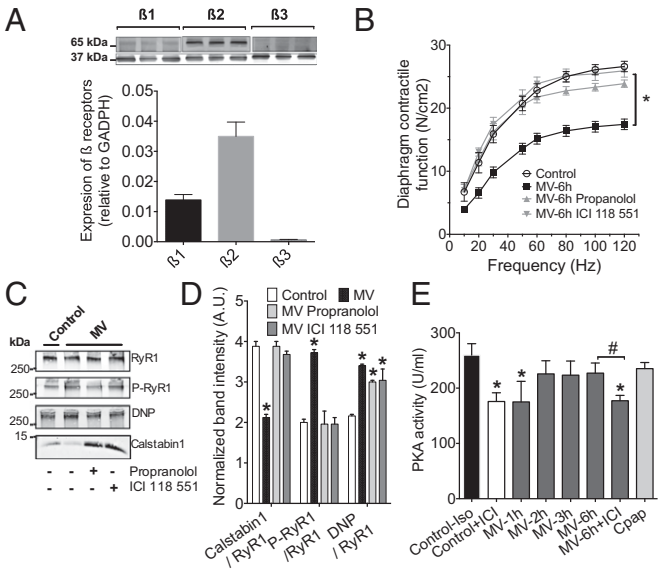

Fig. 4. β-adrenergic pathway is involved in VIDD. (*A*) Representative Western blots and distribution of β-adrenergic receptors in control diaphragm ($n = 6$, $^*P < 0.05$). (*B*) Diaphragm muscle-specific force–frequency relationships recorded in control (Control, $n = 10$), under controlled mechanical ventilation during 6 h (MV, $n = 10$) and MV treated with nonspecific β1-β2 receptor antagonist propranolol (MV-propranolol, $n = 10$), and ICI118551 a β2-adrenoreceptor specific inhibitor (MV+ICI, $n = 10$) ($^*P < 0.05$, MV vs. control and MV-propranolol, and MV-ICI). (*C*) Representative immunoblots and quantification of immunoprecipitated RyR1 from mouse diaphragm samples collected in control ($n = 5$) after 6 h of MV ($n = 5$) and MV in the presence of propranolol ($n = 5$) or ICI118551 ($n = 5$). (*D*) PKA activity was measured in diaphragm muscles treated in mice treated for 30 min with isoproterenol (3 mg/kg, Control+iso), with ICI118551 (10 mg/kg), and after 1, 2, 3, and 6 h of ventilation. In a series of experiments, mice received a first injection of ICI118551 at the onset of anesthesia and 0.7 $mg{\cdot}kg^{-1}{\cdot}h^{-1}$ during the 6 h of MV (MV+ICI). Data are expressed as PKA activity in units per mL, quantified by using a colorimetric assay. Data represent mean ± SEM of 3–6 mice by group. $^*P < 0.05$ compared with Control+iso. $\#P < 0.05$ compared with MV6h (untreated ventilated mice).

Discussion

In the present study, we report that patients under MV with VIDD, and mice subjected to MV, exhibit the biochemical signature of leaky RyR1 channels and evidence of intracellular Ca^{2+} leak. We also demonstrate that this RyR1 dysfunction is driven by β-adrenergic signaling pathway in synergy with MV-induced oxidative stress, which has been extensively studied in VIDD (16). Indeed, RyRs are highly sensitive to oxidative/nitrosative stress in skeletal muscle and in other tissues (25, 32–34). This RyR1 remodeling occurs in other chronic or inherited disease including heart failure (25), diabetes (35), and Duchenne muscular dystrophy (28, 33). Postranslational modification of RyR1 also progresses with aging and partially accounts for age-dependent muscle weakness (27).

In the mouse model, Ca^{2+} sparks frequency is commonly used as an index of RyR1-mediated SR Ca^{2+} leak and is complementary to the biochemical analyses and electrophysiological studies used to demonstrate the contribution of leaky RyR1 in skeletal muscle disorders (27, 28). Therefore, as reported (24, 27, 28), leaky RyR1 may account for a reduction in the Ca^{2+} transient and force production, without the need to invoke other muscle pathology such as atrophy or injury. Indeed, in the VIDD mouse model, we showed a significant level of diaphragmatic muscle weakness without any histological modifications of the muscle after 6 h of MV, supporting the idea that muscle damage or atrophy may not by itself explain VIDD-induced muscle weakness (20). These data suggest that impaired RyR1 function is an early event that precedes muscle damage. Furthermore, early RyR1-dependent defects in intracellular Ca^{2+} homeostasis may be an important mediator of subsequent diaphragmatic muscle remodeling in VIDD as reported in Duchenne muscle dystrophy (28).

To date, oxidative stress was the most documented pathophysiological mechanism accounting for VIDD. The antioxidant Trolox was reported to prevent VIDD in a rat model (8). It was also reported that oxidative stress is required for MV-induced activation of calpain and caspase-3 in the diaphragm (30), but the involvement of Ca^{2+} homeostasis while hypothesized had never been demonstrated. Our data establish that Trolox also prevents RyR1 dysfunction induced by MV in mice. Thus, RyR1 oxidation appears as a prerequisite for RyR1 dysfunction in VIDD. This aspect was further investigated by using the CPAP mode of ventilation to keep the airways continuously open, even in a context of sedation, allowing spontaneous breathing. Respiratory muscles remain active and are not unloaded or passively stretched as they are in MV, a situation that may explain why they are protected under CPAP from VIDD development (26). Interestingly, our CPAP data indicate that maintaining diaphragm activity prevents RyR1 oxidation and VIDD development, even in presence of RyR1 PKA phosphorylation. The origin of ROS production remains unclear during VIDD although recent studies rather consider that mitochondria represent the main source of ROS (10). Recent studies have identified a new transduction pathway in which the microtubule network acts as a mechano-transduction element that activates NADPH-oxidase 2 (Nox2)-dependent ROS generation during mechanical stretch (36). Such pathway could therefore contribute to this primary ROS production. This hypothesis is supported by the beneficial effect of apocynin on the diaphragm during prolonged MV (37). However, we have demonstrated that RyR1

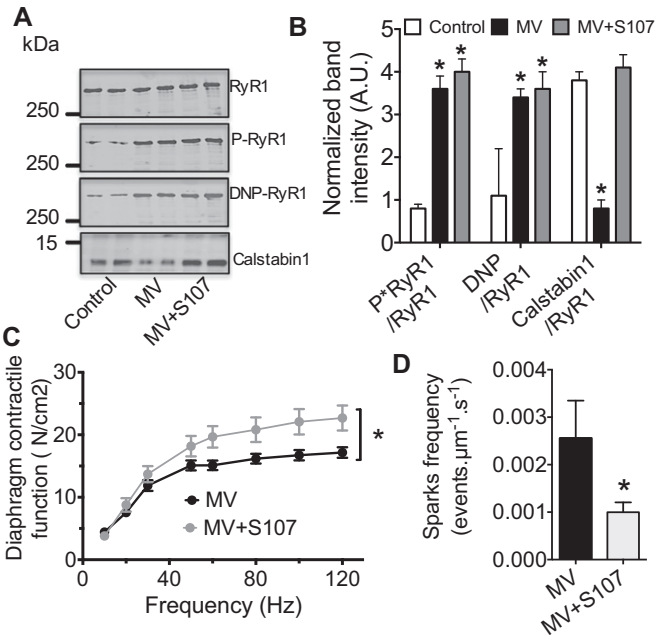

Fig. 5. Reducing RyR1 leak with the Rycal (S107) prevents VIDD after 6 h of MV. Representative immunoblots (*A*) of immunoprecipitated RyR1 from mouse diaphragm samples collected after 6 h of controlled mechanical ventilation with (MV-S107) or without (MV) S107 treatment (75 mg/kg, drinking water). (Each blot corresponds to adjacent wells of the same gel.) Bar graphs (*B*) show quantification of immunoblots, relative to total RyR1 immunoprecipitated. Results are expressed as mean ± SEM, $n = 6$ in control and 5 in MV and MV-S107 groups ($^*P < 0.05$ vs. control). (*C*) Diaphragm muscle-specific force–frequency relationships recorded in MV ($n = 10$) and in MV-S107 ($n = 5$) groups. (*D*) Comparison of mean Ca^{2+} sparks frequency between MV and MV-S107, groups used as an index of resting SR Ca^{2+} leak. Results are expressed as mean ± SEM ($^*P < 0.05$, vs. MV and MV-S107).

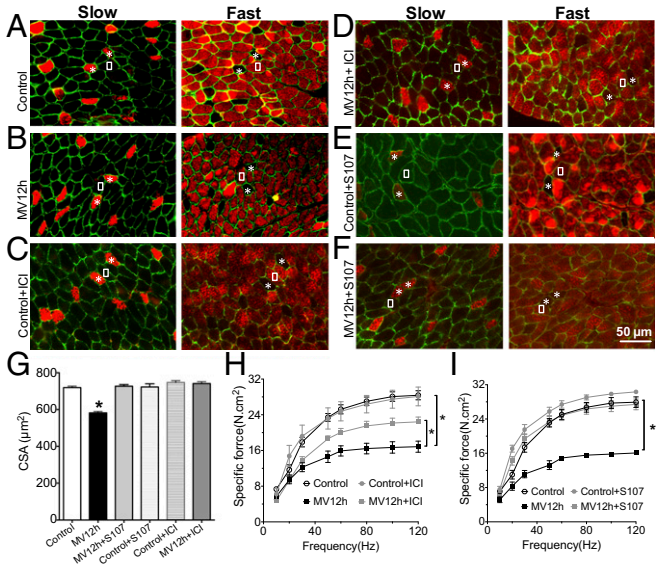

Fig. 6. RyR1 dysfunction contributes to muscle fiber atrophy after 12 h of ventilation. Representative immunostaining of fast and slow diaphragm muscle fibers in mouse. Antibodies against fast- and slow-type myosin ATPase were used to perform immunostaining on cryosections of mouse diaphragm. Muscle membrane was counterstained with dystrophin antibodies. White squares indicate fast fibers, whereas the asterisks show the slow fibers in consecutive sections. Staining was performed in control (control) (*A*), mice under controlled mechanical ventilation during 12 h (MV12h) (*B*), control treated by ICI118551 (Control+ICI) (*C*), control mice treated by S107 (Control+S107) (*D*), mice ventilated during 12 h and treated by ICI118551 (MV12h+ICI) (*E*), and mice ventilated during 12 h and treated by S107 (MV12h+S107) (*F*). (*G*) Quantification of cross-section are in each condition (n = 192–852 fibers for each group, $*P > 0.05$). (*H*) Diaphragm muscle-specific force–frequency relationships recorded in control (n = 7), control+CI118551 (n = 3), MV12h (n = 10), and MV12h+ICI118551 (n = 6) ($*P > 0.05$, MV vs. control and MV12h+ICI). (*I*) Diaphragm muscle-specific force–frequency relationships recorded in control (n = 6), control+S107 (n = 3), MV12h (n = 6), and MV12h+S107 (n = 5) ($*P > 0.05$, MV vs. control and MV12h+S107).

dysfunction and SR-mediated Ca^{2+} leak is also a cause of mitochondrial ROS production (27). We also hypothesized that the phosphorylation status of RyR1 secondary to PKA activation resulted from increased sympathetic tone during anesthesia. Indeed, anesthetic agents such as pentobarbital are known to act as negative inotropic agents and to interfere with the function of the baroreceptor reflexes (38, 39). These systemic effects may therefore contribute to an elevation of endogenous circulating catecholamine during anesthesia although this elevation is so far not clearly documented in ICU patients. Nevertheless, the adrenergic system is known to be overstimulated in patients with critical illness (17, 18). Furthermore, exogenous catecholamines are used to treat cardiovascular instability in critically ill patients (40), amplifying the endogenous catecholamine burst release. This adrenergic burst would support the hypothesis that such stress would be prolonged, becoming maladaptive and exerting adverse effects. The increased level of RyR1 PKA phosphorylation in our human diaphragm samples is in line with this observation. Such β-adrenergic overdrive is consistent with the beneficial effects of β-adrenergic receptor antagonists that we observed (i.e., prevention of muscle weakness and atrophy). Interestingly, both beta blockers prevented RyR1 phosphorylation and depletion of calstabin1 without decreasing RyR1 oxidation. These results combined with those obtained in the CPAP model demonstrate that both RyR1 oxidation and phosphorylation are required to account for the RyR1 dysfunction in VIDD. Given that RyR1 is PKA phosphorylated and oxidized in VIDD, the specific use of β2-adrenergic antagonists could be a potential future target to potentially prevent VIDD. This observation is however in contrast with a recent study showing that low-dose theophylline treatment can significantly improve diaphragmatic movements in patients with VIDD without any significant improvement for weaning time and total ventilation time (41). Theophylline is a methylxanthine that inhibits phosphodiesterases and increase cAMP level as β-adrenergic receptor. This effect could explain in part the positive inotropism that accounts for better diaphragm motion. Because VIDD is known to be one of the major contributors to weaning difficulties, we cannot conclude that theophylline prevents VIDD. Nevertheless, the beneficial effects of beta blockers may not be specifically due to improved RyR1 function and may also have adverse effects. To address this potential lack of specificity, we demonstrate that "fixing" specifically this RyR1-mediated leak with S107 can prevent muscle weakness induced by 6 and 12 h of ventilation in mice. Fixing SR Ca^{2+} leak prevents also changes in a fiber cross-sectional area after 12 h of MV. SR Ca^{2+} leak may contribute to the activation of Ca^{2+}-dependent proteolytic enzymes (caspases and calpains) and Ca^{2+}-dependent regulation of gene expression involved in deleterious muscle injury and wasting processes (42). As mentioned above, RyR is a target in many pathophysiological conditions (21). This finding can be explained in part by the ubiquitous function of Ca^{2+} in cellular processes and by the enormous size of the RyR macromolecular complex and, in particular, its cytoplasmic domain that serves as a redox sensor (43). Therefore, the fact that RyR1 is a potential mediator of muscle weakness in VIDD suggests that patients with comorbidities and/or confounding factors that may affect RyR1 function such as heart failure or aging may have a greater vulnerability to VIDD.

Our mouse model of VIDD has some limitations. First, we used skinned fibers to evaluate Ca^{2+} sparks. This procedure keeps the RyR1 channel in its natural environment but removes the functional interaction with the voltage sensor (L-type Ca^{2+} channels, CaV1.1). Whether a defective RyR1 could negatively regulate other structures involved in intact fibers during excitation–contraction coupling such as CaV1.1 is an interesting question that is beyond the scope of the present study. Second, early events involved in VIDD, with a 6- to 12-h period of controlled mode MV to induce diaphragm weakness in mice, may not be directly applicable to other animal models (20) or to patients on long-term ventilation in the ICU. However, we have recently demonstrated the link between duration of controlled MV and diaphragmatic dysfunction in ICU patients and emphasized the rapid onset of VIDD during MV (2). It is likely that many of the same mechanisms of VIDD are involved across species, although the time course appears to be more protracted in humans. In addition, assisted modes of ventilation, which permit a certain level of diaphragm activity, are likely to mitigate the development of VIDD (44). This observation may explain why CPAP on the basis of RyR1 remodeling does not decrease diaphragm contractile activity (45) and does not induce VIDD. Nevertheless, it remains the case that many patients with acute respiratory distress syndrome or acute brain injury are in fact ventilated in controlled mode, either with or without associated neuromuscular blockade. In this regard, 3 d of controlled mode MV is not uncommon in the ICU and furthermore, additional comorbid factors including sepsis, metabolic disorders, and drugs may even further shorten the latency to VIDD onset (46). VIDD is a major determinant of the ability to successfully wean patients from the ventilator (16, 46). Moreover, we recently reported that diaphragmatic weakness correlates with disease severity and prognosis, suggesting that it is a form of organ failure in ventilated patients (47). Indeed, diaphragmatic weakness normally appears in human after 3–4 d of MV (2). Therefore, any therapeutic strategy, which may prevent this negative evolution, should be considered with a level of great interest.

In conclusion, this study demonstrates the pathophysiological role of RyR1 in VIDD and strongly supports the hypothesis that preventing the RyR1-mediated SR Ca^{2+} leak induced by MV may provide a new therapeutic approach for preventing

diaphragm muscle dysfunction in patients who require artificial respiratory support.

Materials and Methods

Human Model of VIDD. The study in humans was conducted in accordance with the World Medical Association Guidelines for research in humans and approved by the Institutional Ethics Board of the Montpellier University Hospital (protocol NCT00786526). All subjects or their surrogates provided written informed consent to participate in the study.

Murine Model of VIDD. The experimental design has been described in a recent study (20) and has been reviewed and approved by the Animal Care and Use Committee Languedoc-Roussillon and recorded under reference no. CEEA-LR-12078.

Statistics. Data are presented as mean values ± SEM. For biochemical studies and contractile properties, the differences between group means were analyzed by the ANOVA test. Differences in RyR1 open probability were compared by unpaired *t* test with Welch's correction. Statistical significance was defined as $^*P < 0.05$. Detailed methods are presented in *SI Materials and Methods*.

ACKNOWLEDGMENTS. This work was supported by INSERM, Region Languedoc-Roussillon, Association Française contre les Myopathies, the Schaefer Foundation, Philippe Fundation, and the Canadian Institutes of Health Research. G.S. is supported by NIH Grant K99DK107895.

1. Levine S, et al. (2008) Rapid disuse atrophy of diaphragm fibers in mechanically ventilated humans. *N Engl J Med* 358(13):1327–1335.
2. Jaber S, et al. (2011) Rapidly progressive diaphragmatic weakness and injury during mechanical ventilation in humans. *Am J Respir Crit Care Med* 183(3):364–371.
3. Vassilakopoulos T, Petrof BJ (2004) Ventilator-induced diaphragmatic dysfunction. *Am J Respir Crit Care Med* 169(3):336–341.
4. Chang AT, Boots RJ, Brown MG, Paratz J, Hodges PW (2005) Reduced inspiratory muscle endurance following successful weaning from prolonged mechanical ventilation. *Chest* 128(2):553–559.
5. Tobin MJ, Laghi F, Brochard L (2009) Role of the respiratory muscles in acute respiratory failure of COPD: Lessons from weaning failure. *J Appl Physiol (1985)* 107(3): 962–970.
6. Esteban A, et al.; VENTILA Group (2008) Evolution of mechanical ventilation in response to clinical research. *Am J Respir Crit Care Med* 177(2):170–177.
7. Shanely RA, et al. (2002) Mechanical ventilation-induced diaphragmatic atrophy is associated with oxidative injury and increased proteolytic activity. *Am J Respir Crit Care Med* 166(10):1369–1374.
8. Betters JL, et al. (2004) Trolox attenuates mechanical ventilation-induced diaphragmatic dysfunction and proteolysis. *Am J Respir Crit Care Med* 170(11):1179–1184.
9. Powers SK, et al. (2011) Mitochondria-targeted antioxidants protect against mechanical ventilation-induced diaphragm weakness. *Crit Care Med* 39(7):1749–1759.
10. Picard M, et al. (2012) Mitochondrial dysfunction and lipid accumulation in the human diaphragm during mechanical ventilation. *Am J Respir Crit Care Med* 186(11): 1140–1149.
11. Chen M, Won DJ, Krajewski S, Gottlieb RA (2002) Calpain and mitochondria in ischemia/reperfusion injury. *J Biol Chem* 277(32):29181–29186.
12. Belcastro AN, Shewchuk LD, Raj DA (1998) Exercise-induced muscle injury: A calpain hypothesis. *Mol Cell Biochem* 179(1-2):135–145.
13. Jackman RW, Kandarian SC (2004) The molecular basis of skeletal muscle atrophy. *Am J Physiol Cell Physiol* 287(4):C834–C843.
14. Maes K, Testelmans D, Powers S, Decramer M, Gayan-Ramirez G (2007) Leupeptin inhibits ventilator-induced diaphragm dysfunction in rats. *Am J Respir Crit Care Med* 175(11):1134–1138.
15. McClung JM, et al. (2007) Caspase-3 regulation of diaphragm myonuclear domain during mechanical ventilation-induced atrophy. *Am J Respir Crit Care Med* 175(2):150–159.
16. Jaber S, Jung B, Matecki S, Petrof BJ (2011) Clinical review: Ventilator-induced diaphragmatic dysfunction–human studies confirm animal model findings! *Crit Care* 15(2):206.
17. Dünser MW, Hasibeder WR (2009) Sympathetic overstimulation during critical illness: Adverse effects of adrenergic stress. *J Intensive Care Med* 24(5):293–316.
18. Boldt J, Menges T, Kuhn D, Diridis C, Hempelmann G (1995) Alterations in circulating vasoactive substances in the critically ill–a comparison between survivors and nonsurvivors. *Intensive Care Med* 21(3):218–225.
19. Ng Y, et al. (2002) Characterisation of isoprenaline myotoxicity on slow-twitch skeletal versus cardiac muscle. *Int J Cardiol* 86(2-3):299–309.
20. Mrozek S, et al. (2012) Rapid onset of specific diaphragm weakness in a healthy murine model of ventilator-induced diaphragmatic dysfunction. *Anesthesiology* 117(3):560–567.
21. Santulli G, Marks AR (2015) Essential roles of intracellular calcium release channels in muscle, brain, metabolism, and aging. *Curr Mol Pharmacol* 8(2):206–222.
22. Umanskaya A, et al. (2014) Genetically enhancing mitochondrial antioxidant activity improves muscle function in aging. *Proc Natl Acad Sci USA* 111(42):15250–15255.
23. Reiken S, et al. (2003) PKA phosphorylation activates the calcium release channel (ryanodine receptor) in skeletal muscle: Defective regulation in heart failure. *J Cell Biol* 160(6):919–928.
24. Ward CW, et al. (2003) Defects in ryanodine receptor calcium release in skeletal muscle from post-myocardial infarct rats. *FASEB J* 17(11):1517–1519.
25. Santulli G, Xie W, Reiken SR, Marks AR (2015) Mitochondrial calcium overload is a key determinant in heart failure. *Proc Natl Acad Sci USA* 112(36):11389–11394.
26. Bellinger AM, et al. (2008) Remodeling of ryanodine receptor complex causes "leaky" channels: A molecular mechanism for decreased exercise capacity. *Proc Natl Acad Sci USA* 105(6):2198–2202.
27. Andersson DC, et al. (2011) Ryanodine receptor oxidation causes intracellular calcium leak and muscle weakness in aging. *Cell Metab* 14(2):196–207.
28. Bellinger AM, et al. (2009) Hypernitrosylated ryanodine receptor calcium release channels are leaky in dystrophic muscle. *Nat Med* 15(3):325–330.
29. McClung JM, et al. (2008) Redox regulation of diaphragm proteolysis during mechanical ventilation. *Am J Physiol Regul Integr Comp Physiol* 294(5):R1608–R1617.
30. Whidden MA, et al. (2010) Oxidative stress is required for mechanical ventilation-induced protease activation in the diaphragm. *J Appl Physiol (1985)* 108(5):1376–1382.
31. Santulli G, et al. (2012) Age-related impairment in insulin release: The essential role of β(2)-adrenergic receptor. *Diabetes* 61(3):692–701.
32. Donoso P, Sanchez G, Bull R, Hidalgo C (2011) Modulation of cardiac ryanodine receptor activity by ROS and RNS. *Front Biosci* 16:553–567.
33. Fauconnier J, et al. (2010) Leaky RyR2 trigger ventricular arrhythmias in Duchenne muscular dystrophy. *Proc Natl Acad Sci USA* 107(4):1559–1564.
34. Santulli G, et al. (2015) Calcium release channel RyR2 regulates insulin release and glucose homeostasis. *J Clin Invest* 125(5):1968–1978.
35. Turan B, Vassort G (2011) Ryanodine receptor: A new therapeutic target to control diabetic cardiomyopathy. *Antioxid Redox Signal* 15(7):1847–1861.
36. Ward CW, Prosser BL, Lederer WJ (2014) Mechanical stretch-induced activation of ROS/RNS signaling in striated muscle. *Antioxid Redox Signal* 20(6):929–936.
37. McClung JM, et al. (2009) Apocynin attenuates diaphragm oxidative stress and protease activation during prolonged mechanical ventilation. *Crit Care Med* 37(4): 1373–1379.
38. Manders WT, Vatner SF (1976) Effects of sodium pentobarbital anesthesia on left ventricular function and distribution of cardiac output in dogs, with particular reference to the mechanism for tachycardia. *Circ Res* 39(4):512–517.
39. Barker SJ, Gamel DM, Tremper KK (1987) Cardiovascular effects of anesthesia and operation. *Crit Care Clin* 3(2):251–268.
40. Dellinger RP, et al.; International Surviving Sepsis Campaign Guidelines Committee; American Association of Critical-Care Nurses; American College of Chest Physicians; American College of Emergency Physicians; Canadian Critical Care Society; European Society of Clinical Microbiology and Infectious Diseases; European Society of Intensive Care Medicine; European Respiratory Society; International Sepsis Forum; Japanese Association for Acute Medicine; Japanese Society of Intensive Care Medicine; Society of Critical Care Medicine; Society of Hospital Medicine; Surgical Infection Society; World Federation of Societies of Intensive and Critical Care Medicine (2008) Surviving Sepsis Campaign: International guidelines for management of severe sepsis and septic shock: 2008. *Crit Care Med* 36(1):296–327.
41. Kim WY, et al. (2016) Effect of theophylline on ventilator-induced diaphragmatic dysfunction. *J Crit Care* 33:145–150.
42. Petrof BJ, Jaber S, Matecki S (2010) Ventilator-induced diaphragmatic dysfunction. *Curr Opin Crit Care* 16(1):19–25.
43. Eu JP, Sun J, Xu L, Stamler JS, Meissner G (2000) The skeletal muscle calcium release channel: Coupled O2 sensor and NO signaling functions. *Cell* 102(4):499–509.
44. Jung B, et al. (2010) Adaptive support ventilation prevents ventilator-induced diaphragmatic dysfunction in piglet: An in vivo and in vitro study. *Anesthesiology* 112(6):1435–1443.
45. Heulitt MJ, Holt SJ, Wilson S, Hall RA (2003) Effects of continuous positive airway pressure/positive end-expiratory pressure and pressure-support ventilation on work of breathing, using an animal model. *Respir Care* 48(7):689–696.
46. Jung B, et al. (2016) Diaphragmatic dysfunction in patients with ICU-acquired weakness and its impact on extubation failure. *Intensive Care Med* 42(5):853–861.
47. Demoule A, et al. (2013) Diaphragm dysfunction on admission to the intensive care unit. Prevalence, risk factors, and prognostic impact-a prospective study. *Am J Respir Crit Care Med* 188(2):213–219.
48. Fauconnier J, et al. (2011) Ryanodine receptor leak mediated by caspase-8 activation leads to left ventricular injury after myocardial ischemia-reperfusion. *Proc Natl Acad Sci USA* 108(32):13258–13263.
49. Xie W, et al. (2015) Mitochondrial oxidative stress promotes atrial fibrillation. *Sci Rep* 5:11427.
50. Yuan Q, et al. (2016) Maintenance of normal blood pressure is dependent on IP3R1-mediated regulation of eNOS. *Proc Natl Acad Sci USA*, 10.1073/pnas.1608859113.

Supporting Information

Matecki et al. 10.1073/pnas.1609707113

SI Materials and Methods

Human Model of VIDD. The study in humans was conducted in accordance with the World Medical Association Guidelines for research in humans, and approved by the Institutional Ethics Board of the Montpellier University Hospital (protocol NCT00786526). All subjects or their surrogates provided written informed consent to participate in the study.

The study design beneficiated from diaphragm samples obtained during a previous study (2). This first study included two groups of subjects: (*i*) patients with brain death destined for organ donation, who had received MV for at least 24 h before organ harvest (MV, $n = 9$); and (*ii*) patients anesthetized and supported with MV for 2–3 h during thoracic surgery for localized lung nodules (Control, $n = 10$). All subjects were required to have undergone MV via an endotracheal tube in fully controlled mode, i.e., without significant spontaneous breathing efforts during the MV period, with a tidal volume in the average range of 7–8.5 mL/kg of the body weight, respiratory rate from 12 to 24 min, and positive end-expiratory pressure (PEEP) level at 2–5 cmH_2O (2). Diaphragm biopsies (~1 cm^3) were obtained from the zone of apposition of the costal diaphragm at the midaxillary line. In the MV group, the biopsies were obtained before circulatory arrest and removal of other organs. Each biopsy was partitioned and quick frozen in liquid nitrogen and kept at −80 °C. Secondarily, tissue blocks were prepared as required for RyR biochemical and RyR1 functional analysis with single-channel recordings in lipid bilayers as detailed in the last methodology paragraph.

Murine Model of VIDD. The experimental design has been described in a recent study (20) and has been reviewed and approved by the Animal Care and Use Committee Languedoc-Roussillon and recorded under reference CEEA-LR-12078.

In brief, 35 adult male (10–12 wk old, 25–30 g) C57/BL6 mice were separated into three groups.

Mice in the first group were intubated with a 22-gauge angiocatheter and mechanically ventilated for 6 or 12 consecutive hours using a volume-driven small-animal ventilator (Minivent; Harvard Apparatus). Tidal volume was established at 10 μL/mg body weight with a respiratory rate of 150 breaths per min, a PEEP level from 2 to 4 cmH_2O, and a fraction of inspired oxygen of 0.21. Nonspontaneous ventilation was defined as a lack of diaphragm contractile activity attested by repetitive stereotypical deflections observed in the airway pressure curve. The mice mechanically ventilated from this first group were subdivided into 5 subgroups. The first subgroup contained only mice ventilated for 6 (MV) or 12 h (MV12h). The second subgroup was ventilated for 6 h (MV-Trolox) and received a priming dose of Trolox (0.125 mL of saline containing 5 g/L Trolox, corresponding to ~20 mg/kg) i.v. (IV) infused over a 5-min period, 20 min before the start of MV (MV-Trolox). During MV, a constant IV infusion of Trolox at a rate of 4 $mg.^{-1}kg{\cdot}h^{-1}$ (~0.025 mL/h) was maintained. The third subgroup of mice ventilated for 6 h (MV-S107) or 12 h (MV12h+S107) was treated for 7 d before the start of MV, with S107 in their drinking water (final concentration, 0.25 $mg{\cdot}ml^{-1}$) as reported (34, 48, 49) and received the same volume of IV saline 20 min before starting and during MV. The mice drank approximately 3 mL/d (water consumption was variable, and we recorded water bottle and body weight to monitor consumption) for a daily dose of ~0.75 mg (~37.5 $mg{\cdot}kg^{-1}{\cdot}d^{-1}$). The fourth subgroup of mice ventilated for 6 h or 12 h (MV+propanolol, MV12h+propranolol) was treated 30 min before the start of MV with propranolol (3 mg/kg) and one injection every hour. The fifth subgroup of mice ventilated for 6 or 12 h (MV+ICI118551, MV12h+ICI118551) was treated 30 min before the start of MV with ICI118551 (10 mg/kg), respectively, and one injection every hour.

The second group of mice was intubated and treated in an identical manner to the mechanically ventilated mice but breathed spontaneously with a CPAP of 3–4 cmH_2O for 6 h (CPAP). For this purpose, the angio-catheter was connected to an air compressor to deliver a high inspiratory flow rate (1 L/min room air) while the expiratory port was placed under a water seal to obtain PEEP.

All groups mechanically ventilated or under CPAP (first and second group) received the same general care. Mice were anesthetized with i.p. injection of pentobarbital sodium (50 mg/kg body weight) and orally intubated with a 22-gauge angiocatheter. General care applied during the experiments also included continuous reheating by using a homeothermic blanket (Homeothermic Blanket Control unit; Harvard Apparatus, set at 35 °C), and hourly i.p. injection of 0.05 mL of Ringers Lactate solution to maintain hemodynamic stability and compensate insensible losses, as well as bladder expression, eye lubrication, and passive limb movements.

The third group was considered a control group and was divided into three subgroups. The first subgroup was only treated by serum saline (Control, $n = 8$), the second subgroup (Control+ICI118551) was treated with ICI118551 according to the same protocol previously described for the mechanically ventilated mice. The third subgroup (Control+S107) was treated with S107 according to the same protocol previously described for the mechanically ventilated mice. All control mice received the same amount of volume compared with the first group.

Contractile Function in Murine Muscle Samples. At the end of the protocol of MV, the entire diaphragm was surgically excised and mice were euthanized, by exsanguination. Isometric contractile properties were assessed as described in detail (20). The excised diaphragm strip was mounted into jacketed tissue bath chambers filled with equilibrated and oxygenated Krebs solution. The muscles were supramaximally stimulated by using square wave pulses (Model S48; Grass Instruments). The force–frequency relationship was determined by sequentially stimulating the muscles for 600 ms at 10, 20, 30, 50, 60, 80, 100, and 120 Hz with 1 min between each stimulation train (22). After measurement of contractile properties, muscles were measured at Lo (the length at which the muscle produced maximal isometric tension), dried, and weighted. For comparative purposes, diaphragmatic force production was normalized for total muscle strip cross-sectional area and expressed in $N{\cdot}cm^{-2}$. The total muscle strip cross-sectional area was determined by dividing muscle weight by its length and tissue density (1.056 g/cm^3).

The rest of the diaphragm was partitioned: One part was quick frozen in liquid nitrogen and secondarily used for biochemical analysis, and the other part was used freshly for Ca^{2+} spark measurements.

RyR1 Biochemical Analysis. Muscle biopsies were homogenized in 150 μL of buffer containing 5% (wt/vol) SDS, 10% (vol/vol) glycerol, 10 mM EDTA, and 50 mM Tris·HCl buffer (pH 8.0). After centrifugation (8,000 × *g*) at 4 °C, supernatant protein concentrations were measured in duplicate by using the bicinchoninic acid (BCA) protein assay, equilibrated at the same concentration by dilution with loading buffer and aliquoted at

2 μg/μL. RyR1 was immunoprecipitated from 250 μg of homogenate by using an anti-RyR antibody (4 μg of RyR1-1327) in 0.5 mL of a modified RIPA buffer (50 mM Tris·HCl pH 7.4, 0.9% NaCl, 5.0 mM NaF, 1.0 mM Na_3VO_4, 1% Triton X-100, and protease inhibitors) for 1 h at 4 °C. The immune complexes were incubated with protein A Sepharose beads (Amersham Pharmacia) at 4 °C for 1 h, and the beads were washed three times with buffer. Proteins were separated on SDS/PAGE (4–20% gradient) and transferred onto nitrocellulose membranes for 2 h at 200 mA (SemiDry transfer blot; Bio-Rad). To prevent nonspecific antibody binding, the membranes were incubated with blocking solution (LICOR Biosciences) and washed with Tris-buffered saline with 0.1% Tween-20. Blots were respectively incubated with primary antibody to RyR1 (RyR1-1327, an affinity-purified rabbit polyclonal antibody raised against a KLH-conjugated peptide with the amino acid sequence CAEPDTDYENLRRS, corresponding to residues 1327–1339 of mouse skeletal RyR1, with an additional cysteine residue added to the amino terminus), and affinity purified with the unconjugated peptide. We also used antibody to calstabin1 (1:2500 in blocking buffer; LICOR Biosciences); phospho-epitope–specific antibody to human RyR1 phosphorylated on Ser-2808 (1:5000), which detects PKA-phosphorylated mouse RyR1 (on Ser-2844) and RyR2 (on Ser-2808); antibody to S-nitrosylated cysteine residues (1:1000; Sigma). To determine RyR1 oxidation, the immunoprecipitate was treated with 2,4-dinitrophenyl hydrazine, and the derivatized carbonyls were detected by using the OxyBlot protein oxidation detection Kit (catalog S7150; Chemicon International), as described (50). After three washes, membranes were incubated with infrared-labeled secondary antibodies. Control samples were analyzed on each gel for normalization, and total levels of RyR1 were not different between groups.

Ca^{2+} Sparks Measurements. Diaphragm muscles samples were dissected and stored in a Hepes-buffered physiological medium (in mM: 119 NaCl, 5 KCl, 1.25 $CaCl_2$, 1 $MgSO_4$, 10 glucose, 1.1 mannitol, 10 Hepes, pH 7.4). Muscles were then rapidly placed in a dissecting chamber, and the solution was exchanged with a relaxing solution (in mM: 140 K-glutamate, 10 Hepes, 10 $MgCl_2$, 0.1 EGTA, pH 7.0). Bundles of 5–10 diaphragm fibers were manually dissected, mounted as described (23, 24, 28), and permeabilized in a relaxing solution containing 0.01% saponin for 30 s (22). After washing with saponin-free solution, the solution was changed to an internal medium for imaging (in mM): 140 K-glutamate, 5 Na_2ATP, 10 glucose, 10 Hepes, 4.4 $MgCl_2$, 1.1 EGTA, 0.3 $CaCl_2$, Fluo-3 0.05 pentapotassium salt (Invitrogen), pH 7.0, for sparks acquisition as reported (24). Potential sparks were empirically identified by using an autodetection algorithm (24). The mean fluorescence (F0) value for the image was calculated by summing and averaging the temporal F at each spatial location, while ignoring potential spark areas. This F0 value was then used to create a smoothing routine. The potential spark locations were visualized and analyzed for spatiotemporal properties as described (9). Image analysis was performed by using IDL (v5.5; Research System). Statistical comparisons were performed by using an ANOVA test with a significance level set at $P < 0.05$ (Sigmastat; v3.5).

Sarcoplasmic Reticulum Vesicle Preparation. Diaphragms were homogenized on ice in 300 mM sucrose, 20 mM Pipes (pH 7.0) in the presence of protease inhibitors (Roche), and centrifuged at 8,000 rpm (5,900 × g) for 20 min at 4 °C. The following supernatant was ultracentrifuged at 32,000 rpm (100,000 × g) for 1 h at 4 °C. The final pellet containing microsomal fractions enriched in SR vesicles was resuspended and aliquoted in 300 mM sucrose, 5 mM Pipes (pH 7.0) containing protease inhibitors. Samples were frozen in liquid nitrogen and stored at −80 °C.

Single Channel Data from Planar Lipid Bilayer Measurements. Planar lipid bilayers were formed from a 3:1 mixture of phosphatidylethanolamine and phosphatidylcholine (Avanti Polar Lipids) suspended (30 mg/mL) in decane by painting the lipid/decane solution across a 200-μm aperture in a side of a polysulfonate cup (Warner Instruments) separating two chambers. The trans chamber (1 mL) representing the intra-SR (luminal) compartment was connected to the headstage input of a bilayer voltage clamp amplifier (BC-525D, Warner Instruments) and the cis chamber (1 mL), representing the cytoplasmic compartment, was held at virtual ground. Solutions in both chambers were as follows: 1 mM EGTA, 250/125 mM Hepes/Tris, 50 mM KCl, 0.64 mM $CaCl_2$, pH 7.35 as cis solution and 53 mM $Ca(OH)_2$, 50 mM KCL, 250 mM Hepes, pH 7.35 as trans solution. The concentration of free Ca^{2+} in the cis chamber was calculated with WinMaxC program (version 2.50; www.stanford.edu/~cpatton/maxc.html). SR vesicles were added to the cis side, and fusion with the lipid bilayer was induced by making the cis side hyperosmotic by the addition of 400–500 mM KCl. After the appearance of potassium and chloride channels, the cis compartment was perfused with the cis solution. Single-channel currents were recorded at 0 mV by using a Bilayer Clamp BC-535 amplifier (Warner Instruments), filtered at 1 kHz, and digitized at 4 kHz. All experiments were performed at room temperature. Data acquisition was performed by using Digidata 1440A and Axoscope 10.2 software, and the recordings were analyzed by using Clampfit 10.2 (Molecular Devices). Open probability was identified by 50% threshold analysis byusing a least 2 min of continuous record. At the conclusion of each experiment, ryanodine (5 μM) was added to the cis chamber to confirm channels as RyRs.

PKA Activity Assay. Samples were thawed on ice, and PKA activity was determined by using a colorimetric assay (Arbor assay) according to manufacturer's instructions. This assay uses an immobilized PKA substrate bound to a microtiter plate. Briefly, diaphragm samples containing PKA were, in the presence of the supplied ATP, to phosphorylate the immobilized PKA substrate. A rabbit antibody specific for the phospho-PKA substrate binds to the modified immobilized substrate. A secondary antibody specific for rabbit IgG labeled with peroxidase is then added to the plate to bind to the primary rabbit anti-phospho-PKA substrate. After a short incubation and wash, substrate is added and the intensity of the color is directly proportional to the amount of PKA activated in the samples and standards. Samples in the flat-bottom 96-well plate were quantitated by measuring absorbance at 450 and 650 nm by using a microplate reader. A standard curve was obtained by using a cAMP-dependent protein kinase as control.

Statistics. Data are presented as mean values ± SEM. For biochemical studies and contractile properties, the differences between group means were analyzed by the ANOVA test. Differences in RyR1 open probability were compared by unpaired t test with Welch's correction. Statistical significance was defined as $^*P < 0.05$.

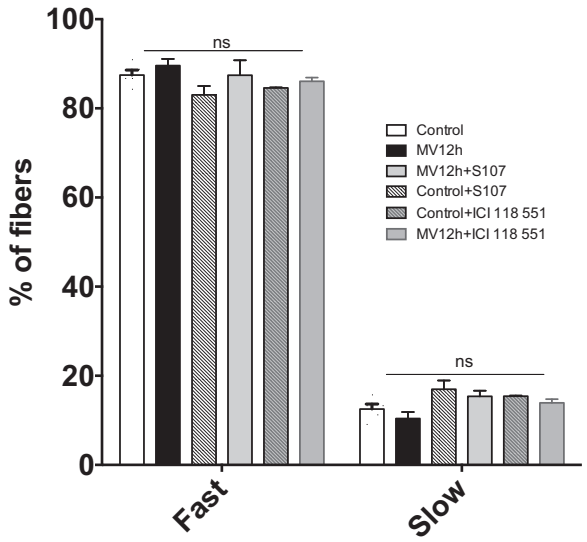

Fig. S1. Fast and slow twitch fibers in diaphragm muscle in control, MV 12 h, control+ICI118551, control+S107, MV12hours +ICI118551, and MV 12hours+S107. (n = 192–852 fibers for each group).

Table S1. Clinical characteristics of patients

Parameters	Short-term MV	Long-term MV
Duration of MV	2.3 ± 0.4	98 ± 65**
No. of patients	10	9
Age, y	53 ± 9	39 ± 19*
Sex, M/F	9/1	3/6
Weight, kg	72 ± 15	74 ± 14
Height, cm	170 ± 10	170 ± 11
BMI, kg/cm^2	25 ± 5	25 ± 3
Reason for surgery/cause of brain death	Stage 1A adenocarcinoma of the lung	Stroke (7), Motor vehicle accident (1), Cardiac arrest (1)

BMI, body mass index; MV, mechanical ventilation. *P < 0.05; **P < 0.01.